Quantified Uniformity and Selectivity of TiO$_2$ Films in 45-nm Half Pitch Patterns Using Area-Selective Deposition Supercycles

Rachel A. Nye, Kaat Van Dongen, Jean-François de Marneffe, Gregory N. Parsons,* and Annelies Delabie*

Area-selective deposition (ASD) shows great promise for sub-10 nm manufacturing in nanoelectronics, but significant challenges remain in scaling to ultrasmall dimensions and understanding feature-dependent nonuniformity and selectivity loss. This work addresses these problems by simultaneously quantifying uniformity and selectivity for passivation/deposition/etch supercycles in 45 nm half-pitch TiN/SiO$_2$ line/space patterns. This work employs three selective processes that are uniquely suited for supercycle processing: dimethylamino-trimethylsilane (DMA-TMS) inhibition, TiO$_2$ atomic layer deposition (ALD), and HBr/BCl$_3$ plasma etch. The DMA-TMS inhibition selectively passivates the SiO$_2$ nongrowth surface without affecting deposition on the TiN and TiO$_2$ growth surfaces. The plasma etch removes TiO$_2$ defect particles at a faster rate than the conformal TiO$_2$ film or SiO$_2$ lines. Using three supercycles of this process, this work demonstrates 8 nm of TiO$_2$ with 88% uniformity and ≈100% selectivity according to transmission electron microscopy (TEM), a 2×improvement in film thickness from previous reports in similar nanoscale patterns. Integrated consideration of uniformity and selectivity at specific feature scales will facilitate the effective design of selective deposition processes for nanoscale electronic devices.

R. A. Nye, K. Van Dongen, J.-F. de Marneffe, A. Delabie
Imec
Kapeldreef 75, Leuven 3001, Belgium
E-mail: Annelies.Delabie@imec.be

R. A. Nye, G. N. Parsons
Department of Chemical and Biomolecular Engineering
North Carolina State University
911 Partners Way, Raleigh, NC 27695, United States
E-mail: gnp@ncsu.edu

R. A. Nye, K. Van Dongen, A. Delabie
KU Leuven (University of Leuven)
Celestijnenlaan 200F, Leuven 3001, Belgium

1. Introduction

Area-selective deposition (ASD) techniques have recently grown significant research interest to enable sub-10 nm resolution in semiconductor manufacturing.[1–3] ASD relies on chemical differences on different regions of a substrate to deposit material at a different rate in each region, thus resulting in bottom-up nanopattern growth.[1,4] Deposition on the desired "growth" region occurs more quickly than on the desired "nongrowth" region and is typically achieved using techniques such as chemical vapor deposition or atomic or molecular layer deposition (ALD/MLD).[1,5] ALD and MLD utilize chemically self-limiting vapor-solid surface reactions of alternating precursors to deposit conformal, pinhole-free films with atomic-scale thickness control and high surface sensitivity.[6–8] These processes have successfully demonstrated ASD of many metals,[9,10] dielectrics,[4,11–14] and organic materials,[5,15,16] resulting in a wide range of applications. For example, TiO$_2$ thin films have a high refractive index, visible and near-IR frequency transmittance, and high chemical stability for use as antireflection coatings, sensors, photocatalysts, and etch resistant layers in lithography stacks,[17–20] and is the focus of our work.

Comparisons between different ASD processes are enabled by a consistent definition of the selectivity fraction, shown in **Equation (1)**, based on the relative surface coverage of material deposited on each surface.[21] Here S represents selectivity and θ and t represent surface coverage and film thickness, respectively, on the growth (G) and nongrowth (NG) surfaces.

$$S = \frac{(\theta_{\text{G}} - \theta_{\text{NG}})}{(\theta_{\text{G}} + \theta_{\text{NG}})} \leq \frac{(t_{\text{G}} - t_{\text{NG}})}{(t_{\text{G}} + t_{\text{NG}})} \tag{1}$$

While inherently selective depositions are possible,[10,22] selectivity is often improved by activating the growth surface[13] or passivating the nongrowth surface.[4,9,23,24] Surface

**ADVANCED
SCIENCE NEWS**

www.advancedsciencenews.com

**ADVANCED
MATERIALS
INTERFACES**
Open Access

www.advmatinterfaces.de

passivation occurs when the nongrowth surface is chemically modified to make it less reactive toward the subsequent ALD process. Alkylsilyl groups have attracted recent attention as passivating groups in ASD for their increased thermal stability, smaller size, and easier process integration (vapor phase, shorter dose time) compared to traditional self-assembled monolayer passivation.[25–29] For example, dimethylamino-trimethylsilane (DMA-TMS) has demonstrated successful passivation of SiO_2 against TiO_2, TiN, Ru,[30,31] and ZrO_2.[32] DMA-TMS reacts efficiently with Si–OH surface groups,[33,34] achieving a TMS site density of ≈2 TMS sites nm^{-2},[30] and thus increasing the hydrophobicity of the surface to inhibit ALD. However, even with inhibitors such as DMA-TMS, surface selectivity is eventually lost.

Further improvement in selectivity has been obtained for some processes using defect mitigation strategies (e.g., etching) or cyclical processes that embed defect mitigation and/or passivation steps into the ALD sequence.[6,35–37] These cyclical processes are especially suited toward improving selectivity on surfaces where undesired nuclei are periodically generated, such as has been recently demonstrated for TiO_2 ASD on DMA-TMS passivated SiO_2.[38] DMA-TMS is uniquely suited for such a cyclic ASD process, as furthermore, it is relatively unreactive on many deposited materials (TiO_2, TiN, and Ru),[31] and therefore may be useful to enable ASD on these surfaces versus SiO_2. The low reactivity of DMA-TMS toward TiO_2 surfaces is in line with the lower surface acidity of TiO_2.[34] Additionally, it has been attributed to more hydrogen bonding occurring on TiO_2 surfaces compared to SiO_2, thus lowering the reactivity of vicinal Ti–OH sites with the inhibitor.[31,34,38,39] However, improving TiO_2 selectivity using DMA-TMS in a cyclic dep/etch cycle has not previously been explored. Therefore, investigating the potential for DMA-TMS to improve selectivity in cyclical ASD is highly desirable.

An additional outstanding challenge in ASD is successfully demonstrating selectivity on feature scales commensurate with current electronic devices. Mechanisms that enable ASD on large (>100 nm) patterns[1] will likely not directly scale to extremely small (<20 nm) features in current commercial devices. Moreover, as feature scales continue to shrink, controlling film uniformity in the vertical direction is essential for complex 3D structures, e.g. fabrication of complimentary field-effect transistors (CFET).[40] Thus, more detailed understanding on pattern-dependent selectivity and uniformity is critical.[41]

Herein we take a significant step forward in sub-50 nm processing using a cyclical TiO_2 ASD process with DMA-TMS as an inhibitor that doubles the best previously achieved TiO_2 film thickness at this scale. Moreover, we specifically investigate selectivity and uniformity in the nanopatterns with a critical dimension (CD) of 45 nm, emphasizing the importance of focusing research efforts on feature-scale processing. In addition, we analyze the pattern dependence of the nonuniformity in the industrially relevant CD range between 2 and 60 nm. The insight obtained in this study provides a new benchmark in the field of nanoscale ASD and demonstrates how understanding fundamental mechanisms is crucial to improving process performance on industrially relevant scales.
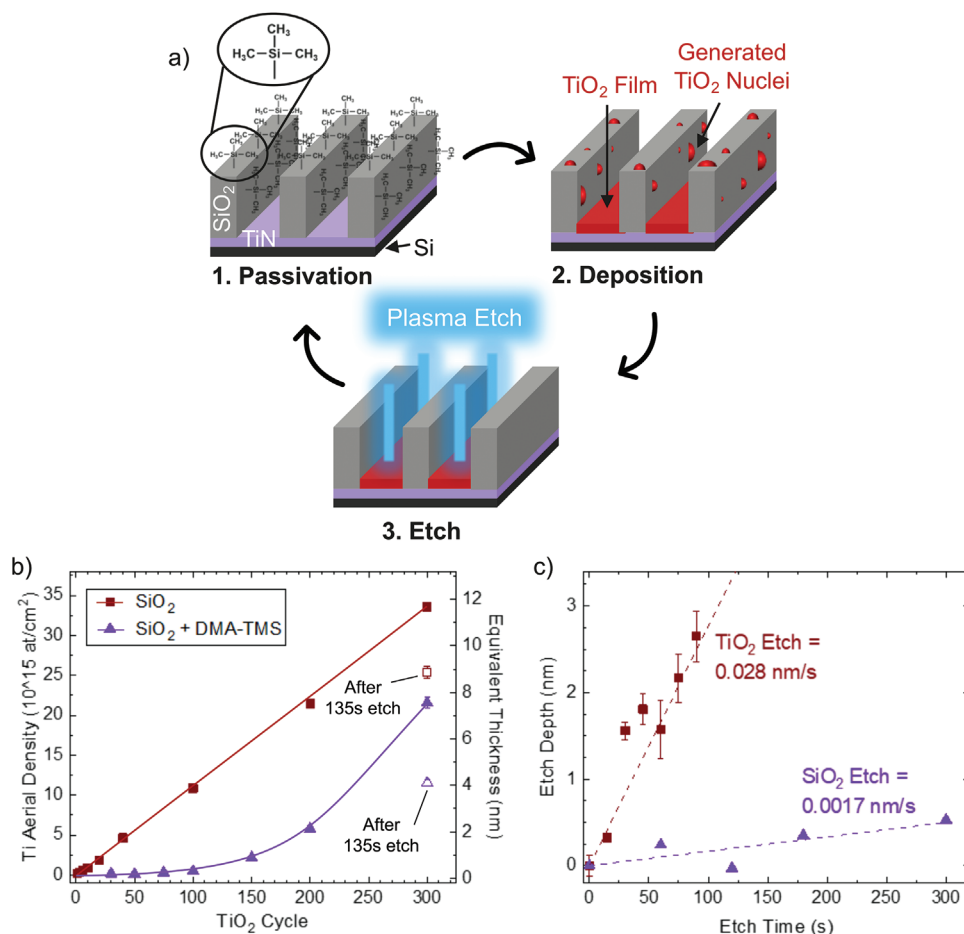
2. Results

2.1. TiO$_2$ Selective Etch with HBr/BCl$_3$ Plasma

In this work, we develop and describe a cyclical passivation + deposition + etch strategy that enables high-selectivity TiO_2 ASD in industrially relevant sub-50 nm patterned features, and utilize the dep/etch sequence to reveal mechanisms leading to feature- and scale-dependent selectivity. The cyclical process is shown in **Figure 1**a, with TiN as the growth surface and SiO_2 as the nongrowth surface. The patterned surface is first exposed to DMA-TMS at 250 °C for 300 s (DMA-TMS partial pressure ≈3 Torr, as described in Experimental Section), which reacts minimally on the exposed TiN, but reacts with hydroxyl sites on the SiO_2 to produce nonreactive Si–O–Si$(CH_3)_3$ sites that passivate the surface and impede TiO_2 nucleation.[31] The sample is then exposed to TiO_2 ALD using $TiCl_4/H_2O$ at 150 °C. Under these conditions on receptive (i.e., unpassivated) SiO_2, the TiO_2 grows at 0.037 nm $cycle^{-1}$ according to Rutherford backscattering spectrometry (RBS) results, as seen in Figure 1b.[38] The Ti aerial density determined from RBS is used to calculate equivalent TiO_2 film thickness assuming a film density of 3.72 g cm^{-3}. On the unpassivated surface, TiO_2 grows at ≈0.037 nm $cycle^{-1}$. After ALD, the sample is treated for a short time with a low-RF power $BCl_3/HBr/Ar$ plasma at 50 °C, without applied substrate bias, that works to etch TiO_2 from both the desired growth and nongrowth regions. Controlling the etch time removes undesired nuclei on the nongrowth surface (i.e., DMA-TMS passivated SiO_2) without completely removing the TiO_2 film from the growth surface (i.e., TiN) or damaging the underlying substrate (SiO_2).

For the etch process, ALD TiO_2 films were exposed to the etch conditions for various times, and the thickness of film etched was measured by ellipsometry. As shown in Figure 1c, the etch depth increases approximately linearly with time, corresponding to an etch rate of 0.028 nm s^{-1}. We also tested the etch process on the passivated SiO_2. For this test, to mimic the SiO_2 surface after the dep/etch sequence, a 50 nm PEALD SiO_2 layer on silicon was pretreated with DMA-TMS. The sample was then exposed to $BCl_3/HBr/Ar$ plasma etching, and the extent of SiO_2 removed was monitored versus etch time. The results in Figure 1c show that on this nongrowth surface, the rate of etching is ≈0.0017 nm s^{-1}, more than 10× smaller than on TiO_2. The difference in etch rates provides an opportunity for a selective etch to aid in removal of undesired TiO_2 without significantly damaging the substrate.

2.2. SiO$_2$ Surface After Passivation, TiO$_2$ ALD, and Etching

To understand reactions on the nongrowth (SiO_2) surface, wafer pieces with thermal SiO_2 were treated with DMA-TMS followed by TiO_2 ALD (50–100 cycles) and $BCl_3/HBr/Ar$ plasma etch (15–90 s), and analyzed by X-ray photoelectron spectroscopy (XPS), water contact angle (WCA), scanning electron microscopy (SEM), and RBS. As shown in **Figure 2**a, the starting SiO_2 + DMA-TMS surface is hydrophobic (WCA = 102°), and the WCA is only slightly decreased (≈89°) after 75 cycles of TiO_2 ALD, consistent with a small amount of TiO_2 growth. Upon etching, the WCA decreases to 21°–25°, equal to that measured on the starting SiO_2, indicating the etch step removes any deposited TiO_2 as well as the underlying passivation layer.

**ADVANCED
SCIENCE NEWS**

www.advancedsciencenews.com

**ADVANCED
MATERIALS
INTERFACES**

Open Access

www.advmatinterfaces.de

Figure 1. a) Schematic of cyclical passivation, deposition, and etch supercycles on dimethylamino-trimethylsilane (DMA-TMS) passivated SiO_2 (non-growth) versus TiN (growth) surfaces. b) Ti aerial density (left y-axis) and equivalent TiO_2 film thickness (right y-axis) as a function of ALD cycle on SiO_2 with and without DMA-TMS passivation. For samples with 300 cycles TiO_2, results are also shown after 135 s etch, as indicated on the figure. c) Etch depth as a function of BCl_3/HBr plasma etch time for TiO_2 (red squares) and DMA–TMS passivated SiO_2 (purple triangles), as measured by ellipsometry. Lines are drawn as guides to the eye.
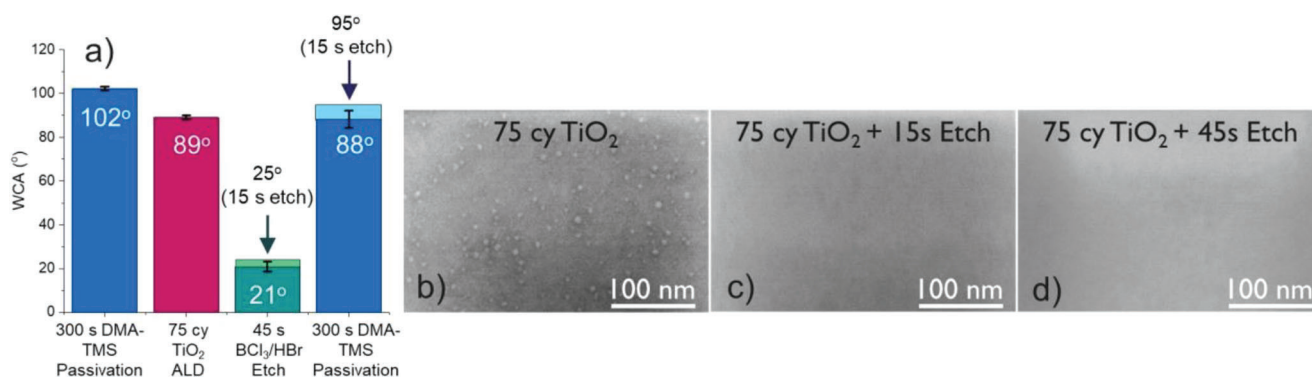
Figure 2. a) Water contact angle (WCA) measurements on an SiO_2 surface after initial 300 s dimethylamino-trimethylsilane (DMA-TMS) passivation, 75 cycles TiO_2 atomic layer deposition (ALD), 15 or 45 s BCl_3/HBr etch, and repassivation with 300 s DMA-TMS after etching. Scanning electron microscopy (SEM) images showing 75 cy TiO_2 on the passivated surface b) before etching, c) after 15 s etch, and d) after 45 s etch.

**ADVANCED
SCIENCE NEWS**

www.advancedsciencenews.com

**ADVANCED
MATERIALS
INTERFACES**

www.advmatinterfaces.de

Table 1. Ti content determined from Rutherford backscattering spectrometry (RBS) for various deposition + etching conditions on SiO_2 and dimethylamino-trimethylsilane (DMA-TMS) passivated SiO_2.

Process	Passivation	Total ALD cycles	Total etch time [s]	Ti content (10^{15} Ti at cm^{-2})
ALD only	None	150	0	16.2 ± 0.2[a]
Passivation + ALD	DMA-TMS	150	0	2.2 ± 0.3
[Passivation + ALD + Etch] × 2	DMA-TMS	150 (75 × 2)	30 (15 × 2)	0.2 ± 0.1
[Passivation + ALD + Etch] × 2	DMA-TMS	150 (75 × 2)	90 (45 × 2)	0.4 ± 0.1

[a] Interpolated from data after 100 and 200 cycles.

Indeed, SEM images in Figure 2b–d show that after DMA-TMS treatment, 75 cycles of TiO_2 ALD produce visible nuclei, and nuclei are not present after 15 or 45 s of etching. XPS results in Figure S1 and Table S1 (Supporting Information) also show removal of TiO_2. For some samples, the etched surfaces were exposed again to 300 s DMA-TMS. As shown in Figure 2a, after 15 s etch, the DMA-TMS exposure reproduced a hydrophobic surface (WCA = 95°). The same trend is observed after 45 s etching, with WCA = 88°. This confirms that DMA-TMS can successfully react with the etched SiO_2 surface and restore the TMS surface termination. We note that further investigation is required to fully elucidate the effects of surface etching (e.g., etch time) on surface repassivation.

2.3. Cyclical Passivation + Deposition + Etch Process on Blanket Wafers

Using the HBr/BCl_3 plasma etch process described above, we evaluated several cycles of the fully integrated passivation + deposition + etch process. For this experiment we analyze an SiO_2 sample after 75 cycles of ALD only and compare it to samples treated as shown in Figure 2, (i.e., 300 s DMA-TMS passivation, 75 cy TiO_2 ALD at 150 °C, and 15 or 45 s etch time). Results from RBS and WCA analysis are given in **Table 1** and Figure S2 (Supporting Information), respectively. The sample exposed only to ALD shows substantial Ti deposition, consistent with facile nucleation and growth, whereas very little Ti is present after the cyclic passivation + deposition + etch, indicating impeded nucleation and removal of unwanted growth. The WCA results after the multistep sequence are also consistent with the single supercycle results in Figure 2. Based on these results, to explore feature dependence in ASD, the passivation + deposition + etch conditions were fixed at 300 s DMA-TMS + 75 cycles TiO_2 ALD + 45 s BCl_3/HBr plasma etch, unless otherwise noted.
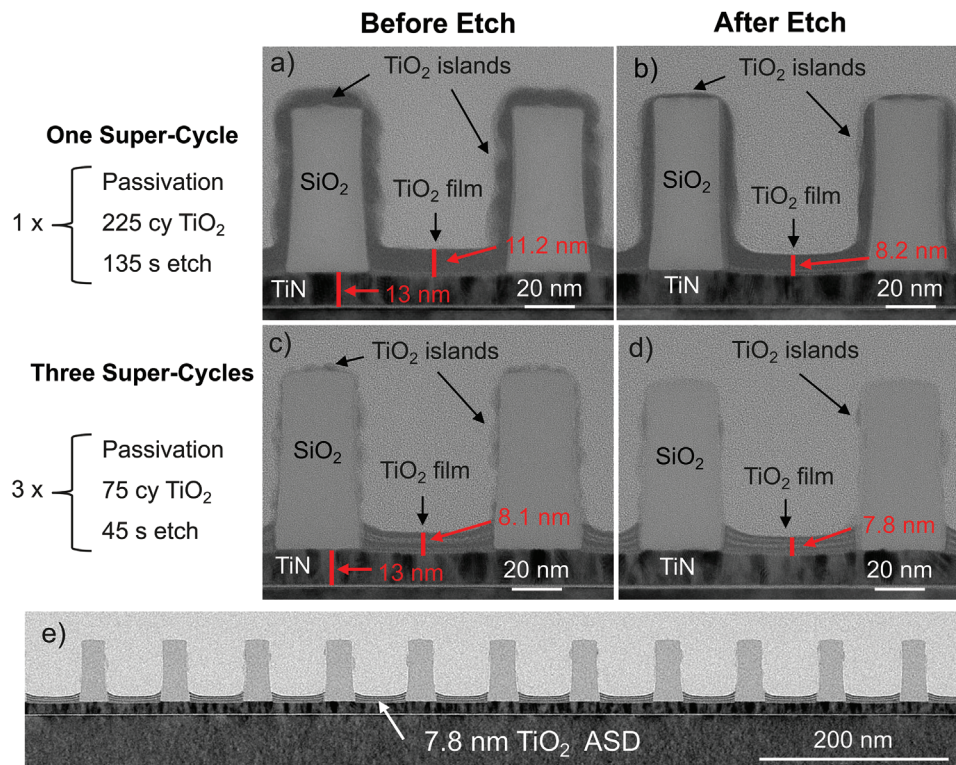
2.4. Demonstrating Selectivity on Nanopatterns

To analyze ASD in nanoscale features, 45 nm half-pitch SiO_2/TiN line/space patterns were prepared using immersion lithography on full wafers and cut into ≈2 × 2 cm^2 coupons before transfer to the reactor for DMA-TMS passivation + ALD + etching using conditions developed above on blanket coupons. For this pattern, the TiN is expected to react minimally with the DMA-TMS passivation, and therefore be receptive to TiO_2 growth, whereas the

DMA-TMS will readily passivate the SiO_2 regions and impede nucleation.[31,38] All samples receive the same ALD treatment (225 cycles) and etch time (135s), but some are processed using one supercycle (consisting of 300 s DMA-TMS passivation + 225 ALD cycles + 135 s etching) while others are processed using three supercycles (i.e., [300 s DMA-TMS passivation + 75 ALD cycles + 45 s etching] × 3). We note that TiO_2 is not inherently selective to SiO_2, in accordance with previous results on blankets,[31,38] supporting the need for the DMA-TMS inhibitor to obtain good selectivity. To analyze the deposition and etching, some samples are removed from the reactor after deposition (without etching). Samples are analyzed using transmission electron microscopy (TEM) with energy-dispersive X-ray spectroscopy (EDS), SEM, and cross-sectional SEM images.

Figure 3a,b shows TEM images of patterned samples after 225 ALD cycles and 225 ALD + 135 s etching, respectively, with the thicknesses of relevant layers reported in **Table 2** and Table S2 (Supporting Information). After ALD only (Figure 3a), the TiO_2 layer on TiN is ≈11.2 nm thick. This is consistent with ≈3 nm of native TiO_2 on the TiN, plus ≈8 nm of TiO_2 ALD formed at the expected 0.037 nm cycle^{-1} measured on blanket substrates (Figure 1b). The thickness is uniform and consistent for 11 different spaces (Figure S3, Supporting Information). Less TiO_2 (≈6.5 nm on average) is also present on the exposed SiO_2 top surface and trench sidewalls, consistent with nucleation inhibition. After 135 s etching (Figure 3b), the average TiO_2 thickness on the top and side of the SiO_2 lines is ≈1.8 and ≈4.9 nm, respectively, indicating that TiO_2 islands on the top surface etch faster than on the sidewalls. On the TiN region, the etching reduces the TiO_2 thickness to ≈8.1 nm in the center of the feature, which is reasonably close to the 7.4 nm expected with an etch rate of 0.028 nm cycle^{-1} (from Figure 1c). Note that after etching, the TiO_2 film thickness in the TiN region is larger near the SiO_2 trench wall (whereas it was uniform before etch), consistent with shadowing during the plasma etch process.

Similar TEM images from samples prepared with three cycles of passivation + deposition + etch are shown in Figure 3c,d, where the sample in Figure 3c was removed before the final etch step. Before the final etch (Figure 3c) the TiO_2 layer thickness on the TiN growth surface is ≈8.1 nm, which is consistent with the ≈8.8 nm expected using the deposition[38] and etching rates on blankets (Figure 1), including a 3 nm native TiO_x layer. In this case, the nonuniformity of the TiO_2 thickness on TiN is somewhat more pronounced than after the single supercycle results

**ADVANCED
SCIENCE NEWS**

www.advancedsciencenews.com

**ADVANCED
MATERIALS
INTERFACES**

www.advmatinterfaces.de

Figure 3. Transmission electron microscopy (TEM) images of patterned samples after a,b) one supercycle and c,d) three supercycles before and after the final etch steps. Total 225 cycles TiO_2 and 135 s etch times are used for each process. Each passivation step is 300 s dimethylamino-trimethylsilane (DMA-TMS) at 250 °C. e) Large area image of sample from (d) to see multiple lines/spaces.

Table 2. Measurements of various dimensions on standard and supercycle patterned wafers from Figure 3.

Process					TiO_2 Thickness [a] (on TiN)/Particle height (on SiO_2) [nm]				
Supercycles	Passivation	Total ALD cycles	Total etch time [s]	On planar TiN (Theoretical) [b]	On patterned TiN (TEM, center)	On patterned TiN (TEM, edge)	On SiO_2 top surface (TEM)	On SiO_2 sidewalls (TEM)
1	DMA-TMS (1×)	225 (225 × 1)	No etch	11.3	11.2 ± 0.2	12.9 ± 0.8	6.6 ± 0.5	6.3 ± 1.3
1	DMA-TMS (1×)	225 (225 × 1)	135 (135 × 1)	7.5	8.2 ± 0.7	13.0 ± 0.5	1.8 ± 0.3	4.9 ± 0.7
3	DMA-TMS (3×)	225 (75 × 3)	90 (45 × 2)	8.8	8.1 ± 0.4	12.7 ± 1.4	1.7 ± 0.7	2.0 ± 0.8
3	DMA-TMS (3×)	225 (75 × 3)	135 (45 × 3)	7.5	7.8 ± 0.6	12.4 ± 0.8	Below detection limit	Isolated particles: 1–3 nm height

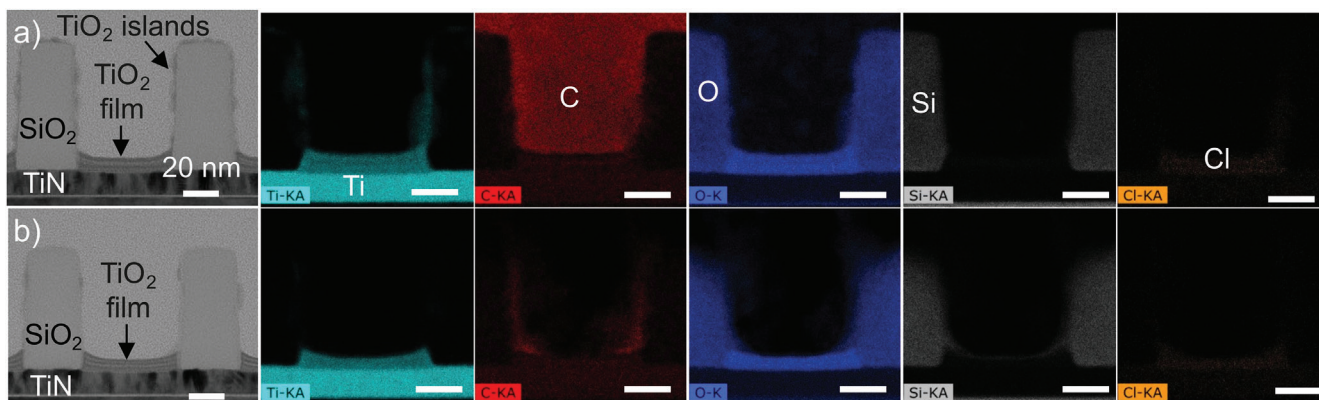[a] Including ≈3 nm native TiO_x. [b] Calculated from growth and etch rates on planar substrates, determined in Figure 1.

in Figure 3b (see also Figure S5, Supporting Information). The average height of the TiO_2 islands on the SiO_2 top surface and sidewalls is ≈1.7 and 2.0 nm, respectively, which is much thinner than the single supercycle sample (Figure 3b).

After three full passivation + deposition + etch cycles, (Figure 3d), the average thickness of the TiO_2 layer on the TiN is ≈7.8 nm, which is reasonably close to 6.8 nm TiO_2 expected after 45 s etching of the 8.1 nm film. On the SiO_2 region, few isolated particles (≈1–3 nm in height) are observed on the sidewalls with TEM, and no defects are observed on the SiO_2 top surface. Also, the width of the SiO_2 feature is not affected by the etching (Table S2, Supporting Information).

Figure 3e and Figure S3 (Supporting Information) show an extended broad view of the patterned sample after three cycles of (passivation + deposition + etch), demonstrating the consis-

tency of the TiO_2 film thickness and selectivity across a large area of the pattern. For the results in Figure 3d, the three supercycle process enables ≈7.8 nm of selective TiO_2 growth on TiN, which is ≈2x larger than previously reported for TiO_2 ASD on similar patterns.[31]

Figure 4a,b shows EDS scans collected from samples in Figure 3c and d, respectively. A Ti-containing (TiO_2) layer is apparent on the TiN. In Figure 4a before the final etch, some Ti signal is also present on the SiO_2 sidewalls, with no measurable Ti on the SiO_2 top surface. Within the TiO_2 layer on the TiN in each sample, small horizontal contrasting layers are observed, which may be related to changes in C content (as observed in Figure 4) or film crystallinity, although low temperature (i.e., 150 °C) TiO_2 deposition is typically expected to produce amorphous films. The C observed within the TiO_2 film is attributed to some residual

**ADVANCED
SCIENCE NEWS**

www.advancedsciencenews.com

**ADVANCED
MATERIALS
INTERFACES**

www.advmatinterfaces.de

Figure 4. Transmission electron microscopy (TEM) energy-dispersive X-ray spectroscopy (EDS) images of three supercycle deposition process a) before and b) after the final etch step. Area-selective deposition (ASD) sequence included 3 × [300 s dimethylamino-trimethylsilane (DMA-TMS) passivation, 75 cy TiO_2 atomic layer deposition (ALD), and 45 s etch]. Color code is as follows: Ti (light blue), C (red), O (dark blue), Si (white), and Cl (orange). All scale bars are 20 nm.
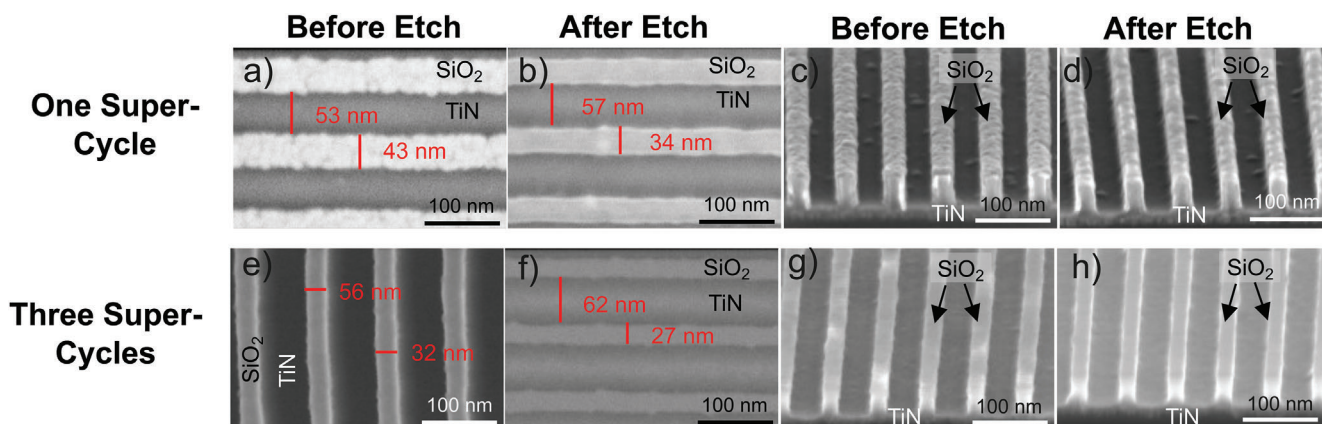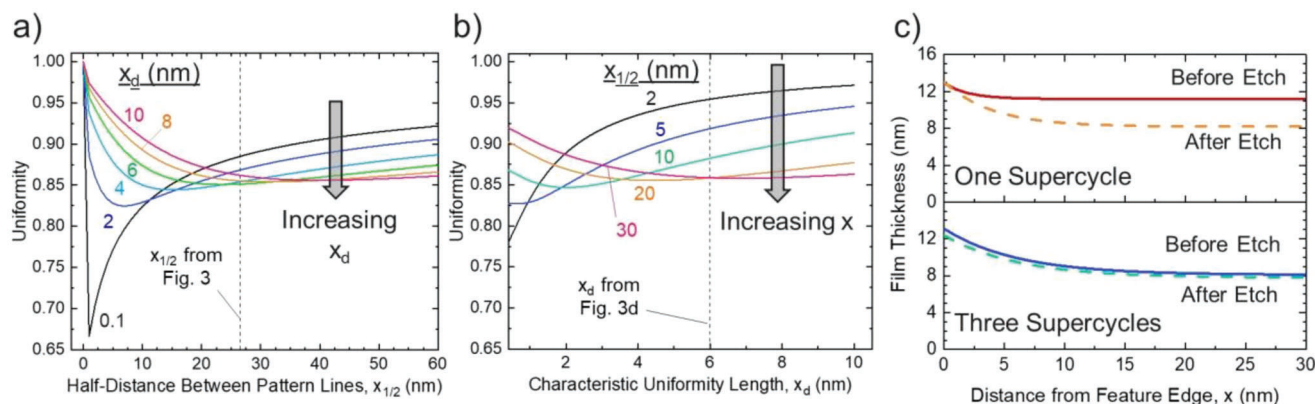

Figure 5. Scanning electron microscopy (SEM) (a,b,e,f) and cross-section SEM (c,d,g,h) images of samples after a–d) one supercycle and e–h) three supercycles before a,c,d,g) and after b,d,f,h) final etch steps, as labeled. Total 225 cycles TiO_2 and 135 s etch times are used for each process. Each passivation step is 300 s dimethylamino-trimethylsilane (DMA-TMS) at 250 °C.

TMS groups on the TiO_2 surface during the repeated passivation steps.[31,42]

After the final etch step (4b), the thickness of the Ti layer on the growth surface has decreased (while maintaining the "U"-shaped profile), and no Ti is visible on the SiO_2 top surfaces or sidewalls. There is a small native SiO_x layer formed on top of the TiO_2 film on the TiN growth surface, which may be attributed to residue from the slowly etched Si lines, residual inhibitor species, or Si-containing residues from intermediate etch processes. Some Cl is observed within the TiO_2 film for both samples, attributed to residual $TiCl_4$ precursor incorporated into the deposited film. No Br (Figure S4, Supporting Information) is detected, consistent with XPS results in Table S1 (Supporting Information). Additionally, we note that there is no increase in defectivity near the corners of the SiO_2 lines using this supercycle process with DMA-TMS, in contrast to previous TiO_2 selectivity studies in similar patterns.[23]

Figure 5 shows top-view and cross-section SEM images of the samples presented in Figure 3. Significant TiO_2 particle defectiv-

ity is observed for the single supercycle process on both the SiO_2 top surface (Figure 5a) and sidewalls (Figure 5c). The line edge roughness (LER) appears quite high before etching for these samples, which is an indicator of island-type nucleation on the sidewalls. While the extent of observed particles and excess SiO_2 line width are significantly reduced after etching (Figure 5b,d), significant LER still remains, which can be problematic for future processing steps. On the contrary, for the three supercycle process, minimal TiO_2 particles are observed on the SiO_2 lines after 225 cycles TiO_2 deposition even before the last etch step (Figure 5e,g). In this case, the pattern edges are significantly smoother than in the standard process, consistent with less sidewall defectivity. After the last etch from the third supercycle, no TiO_2 particles are observed on the SiO_2 top surfaces and little to no defects are observed on the sidewalls (Figure 5f,h). Corresponding line widths are reported in Table S3 (Supporting Information). A more detailed, quantitative analysis of LER during ASD in patterns merits further investigation outside the scope of this work.

ADVANCED
SCIENCE NEWS
www.advancedsciencenews.com

ADVANCED
MATERIALS
INTERFACES
Open Access
www.advmatinterfaces.de

Figure 6. Film uniformity for the cyclical TiO_2 process developed here in patterns as a function of a) half-distance between pattern lines ($x_{1/2}$) and b) characteristic uniformity length (x_d). Vertical dashed lines correspond to the space half-width and characteristic uniformity length used in our experiments in Figure 3d. c) Thickness profiles for deposited TiO_2 film from images in Figure 3, with associated modeling parameters and uniformity provided in Table S4 and Figure S5 (Supporting Information).

2.5. Quantifying Uniformity in Nanopatterns

Using cyclical passivation-deposition-etch as a reliable ASD process in nanopatterns, we next investigate feature dependence of uniformity. To begin to quantify the uniformity of the resulting ASD film, we note that based on the experimental results in Figures 3 and 4, the film thickness is largest near a feature edge, and the thickness decays exponentially with the distance away from the feature. This trend is represented by **Equation (2)**:

$$t(x) = (t_o - t_\infty) * e^{-x/x_d} + t_\infty \tag{2}$$

where $t(x)$ is the film thickness (nm) at any distance (x, nm) away from the feature edge (in this case the SiO_2 line). The values t_0 and t_∞ are the film thicknesses at the SiO_2 line (e.g., $x = 0$) and at a point far away from any edge or feature, respectively. The parameter x_d is a "characteristic uniformity length" representing the extent of thickness change with distance away from the feature, where higher x_d indicates a more rapid change in thickness (from t_o to t_∞) when moving away from the feature edge. Parameters for each image from Figure 3 are provided in Table S4 (Supporting Information), with overlaid thickness profile fits and TEM images shown in Figure S5 (Supporting Information). We assume that the thickness profile is symmetric from the center of the space in this analysis.

Furthermore, the net uniformity, U, of a nonplanar film can be defined as:

$$U = 1 - \frac{\sigma}{t_{avg}} \tag{3}$$

where σ is the standard deviation of film thicknesses (nm), and t_{avg} is the average film thickness (nm). Following this definition, if the thickness of a film is independent of location, then σ approaches zero and $U = 1$, i.e., uniformity equals 100%. By assuming a value for one-half of the feature separation distance, $x_{1/2}$, (i.e., one-half the distance between SiO_2 lines), Equation (2) can be used to determine σ and t_{avg}. Therefore, we can predict how U will depend on t_o, x_d, and $x_{1/2}$ for the $TiCl_4/H_2O$ process.

Results are shown in **Figure 6**. In this figure, the space half-width and characteristic uniformity length corresponding to our experimental patterns (Figure 3d, $t_0 = 12.4$ nm, $t_\infty = 7.8$ nm, and $x_d = 6$ nm) are indicated by the vertical dashed lines. In these plots, U is calculated from Equations (2) and (3), where t_{avg} is determined from Equation (2) using the experimentally determined thickness values, t_0 and t_∞ (listed in Table S4, Supporting Information).

Figure 6a is a plot of uniformity versus feature spacing dimension for various values of x_d, and Figure 6b plots uniformity versus x_d for various feature spacings. The uniformity for etched samples is similar ($\approx 88\%$) after the final etch for both one and three supercycles (Table S4, Supporting Information). From Figure 6a,b, for larger pattern dimensions, uniformity is higher when x_d is small, consistent with the nonuniformity being localized over only a small fraction of the deposition region. For smaller pattern dimensions, uniformity is higher when x_d is large, consistent with a more gradual change in film thickness over the width of the pattern. The lowest uniformity is obtained when pattern dimension is similar to x_d, because in this case the film thickness is changing significantly over a large portion of the pattern. Thus, the best uniformity is obtained with smaller x_d values for large patterns, and with larger x_d values for small patterns. We note the geometric constraint in the observational model as x_d approaches zero that causes a significant drop in uniformity (resulting in a local minimum) for very small pattern dimensions. This result demonstrates the potential negative impact of shadowing effects during etching for very small feature sizes and the limitations of the current model. However, the model provides meaningful insight for larger x_d values or for small x_d values with practical pattern dimensions (i.e., larger than 1 nm half-distance between features).

Figure 6c shows the thickness profiles from TEM images (Figure 3) calculated from Equation (2) and using thicknesses from Table 2 and Figure S4 (Supporting Information). From Figure 6c and Table S4 (Supporting Information), we see that film uniformity decreases significantly after etching for samples processed with only one supercycle (e.g., etch periodicity = 1). In contrast, when increasing the etch periodicity (i.e., after three

**ADVANCED
SCIENCE NEWS**

www.advancedsciencenews.com

**ADVANCED
MATERIALS
INTERFACES**
Open Access

www.advmatinterfaces.de

supercycles with a more frequent, shorter etch step), the uniformity is maintained and slightly improves after the final etching step. The improvement in uniformity for samples processed with more periods of passivation/deposition/etch supercycles is attributed to fewer particles on the sidewalls during this processing, leading to a larger area of the bottom film that is continuously exposed to the etch (i.e., resulting in a similar etch rate across the entire film). On the other hand, increased TiO_2 sidewall deposition (e.g., for longer deposition cycles between etching, Figure 3a,b) results in shadowing of a larger portion of the bottom film during the etching process, causing a lower effective etch rate at the feature edge compared to the feature center. Therefore, to achieve a more uniform film with high selectivity, supercycles with more frequent etching (i.e., higher periodicity) are desirable, consistent with the TEM observations for one versus three supercycles (Figure 3).

Overall, these results indicate the large impact of pattern dimension and processing on uniformity. Note that future work could relate the uniformity model discussed above to supercycle processing conditions to predict the deposited film thickness profile, for example using a nucleation and growth model. As one example, t_∞ and t_0 could be calculated from the ALD growth rate as well as the etch rate at the feature center and edge, respectively. Similarly, x_d could be related to the difference between t_∞ and t_0, the feature width/height, and etch periodicity. This predictive modeling could facilitate supercycle process design to optimize uniformity without compromising selectivity.

3. Discussion

3.1. Recovery of Selectivity by Supercycles with DMA-TMS and Selective Etching

Understanding the impact of etching on the nongrowth surface (including effect of etch reactants, etch time, residue, and changes to surface chemistry and active site density) is crucial for design and optimization of supercycle ASD processes. In this work, etching the DMA-TMS passivated surface with TiO_2 nanoparticles not only removes the TiO_2 nanoparticles but also degrades the TMS layer to expose the original Si–OH surface termination, as indicated by the drop in contact angle after etching observed in Figure 2 and Figure S2 (Supporting Information). This could occur, for example, by etching of the TMS layer by HBr/BCl_3 via formation of volatile etched species such as $SiCl_x(CH_3)_y$, $SiBr_x(CH_3)_y$, $SiCl_x$, $SiBr_x$, CCl_x, or CBr_x, resulting in exposure of the Si–OH substrate surface. The smaller contact angle (Figure 2 and Figure S2, Supporting Information) after re-applying the inhibitor to the etched surface is attributed to residual etch contaminants (e.g., B) or slight damage to the slowly etched SiO_2 surface (e.g., decreased OH content), as observed by XPS in Figure S1 (Supporting Information), which could provide fewer sites for TMS groups to bind and passivate the surface. In order to make the repassivation more efficient, one could consider adding an in situ post-etch surface conditioning aiming to remove residual etch contaminants and/or rehydroxylate the surface. Further investigation into the affect of HBr/BCl_3 etching on the TMS-terminated SiO_2 surface would benefit the repassivation effectiveness and hence improve selectivity.

Importantly, the etch process reliably removes TiO_2 nanoparticles on the passivated surface without completely removing the deposited, conformal film on the growth surface, as confirmed by XPS, TEM, and EDS results in Figure S1, Figures 3, and 4, respectively. TEM (Figure 3), TEM EDS (Figure 4), and SEM (Figure 5) images are consistent in demonstrating significantly less TiO_2 on the passivated surfaces (i.e., SiO_2 top-surface and sidewalls) for depositions that incorporated periodic short etches instead of one long etch. This is expected if the etch removes smaller particles more easily than larger particles, and explains the lower TiO_2 particle coverage on SiO_2 lines (TEM, Figure 3) and the thinner SiO_2 linewidths (SEM, Figure 5) during the three supercycle process compared to the single supercycle process. While higher periodicity has demonstrated reduced defects and improved selectivity in this case, it is also possible that the composition of the deposited film (i.e., TiO_2) is affected by the supercycles (as evidenced by the contrast layers in TEM in Figure 3c,d). It will be important to further investigate the potential impact of supercycles on film properties (e.g., dielectric constant, refractive index, etch resistance, or crystallinity) for applications.

Our previous work demonstrated that the TiO_2 nuclei are continuously generated on DMA-TMS passivated SiO_2 during ALD, and hypothesized that periodic removal of generated defect sites could improve selectivity.[38] Together, the controllable TiO_2 etch and selective DMA-TMS passivation step are well-suited for such a cyclical ASD process. Our current work confirms this hypothesis, as the periodic, load-dependent etching removes the generated TiO_2 particles while they are still small. This enables successful repassivation of the surface and leads to a 2× improvement in selectivity in nanopatterns compared to previous TiO_2 ASD in similar patterns.[23,31] The ≈8 nm TiO_2 film deposited in this work is similar in thickness to other TiO_2 supercycle ASD processes, while we expand our results to smaller pattern sizes and quantify uniformity in the patterns.[6] Our results emphasize the importance of cycling the DMA-TMS passivation, deposition, and etch steps in improving selectivity, and provide an important example of how greater understanding on selectivity loss can improve ASD strategies in sub-50 nm patterns. Further optimization of the etch step and supercycle periodicity are desired to further reduce defectivity.

3.2. ASD Mechanism and Uniformity in Nanopatterns Versus Blankets

The overall deposition and etching processes described here behave somewhat differently on 3D patterns versus planar blanket substrates. This has important implications in transferring research insights to commercial applications, thus we specifically discuss relevant selectivity mechanisms on the nanopatterns. For the patterned samples shown in Figure 3, the same net deposition and etching time result in approximately the same TiO_2 film thickness on TiN, regardless of using one or three supercycles. Thus, the deposition and etch rates on the patterns (Figure 3) are consistent with those measured on blanket wafers (Figure 1). However, for both patterned samples, the TiO_2 film on the TiN region is not completely uniform, with a slightly thicker film on the edges adjacent to the SiO_2 lines.

2300163 (8 of 11)

**ADVANCED
SCIENCE NEWS**

www.advancedsciencenews.com

**ADVANCED
MATERIALS
INTERFACES**
Open Access

www.advmatinterfaces.de

Since the "U"-shape is more pronounced after the etching step, the nonuniformity is attributed to slower TiO_2 etching in the region adjacent to the SiO_2 due to shadowing effects, rather than diffusion of adsorbed species from the passivated sidewalls down to the TiN growth surface.[41] The lack of diffusion is further supported by the lack of a TiO_2 "depletion zone" near the SiO_2/TiN interface (TEM images in Figure 3), which would be expected if Ti-adspecies were diffusing away from the passivated SiO_2 sidewalls and onto the TiN (thereby causing the TiO_2 film thickness to be larger at the pattern edges). Results from Figure 6 demonstrate how this nonuniform profile depends greatly on the pattern dimensions (feature spacing and height). Depending on the x_d value, uniformity may either increase or decrease with smaller pattern dimensions. Thus, characterizing the thickness profile and determining x_d for a given process will be an important indicator for the success of further device scaling.

We can also use CD measurements from SEM images to compare TiO_2 etch rates on the sidewalls during the one and three supercycle process, as supported by consistent line width measurements between TEM (Figure 3) and SEM (Figure 5). We note the ongoing challenges in direct quantitative comparisons due to limitations in metrology for ASD processes. For example, slight tapering of the SiO_2 lines is observed in the TEM images (Figure 3), which may cause deviations in CDs measured between TEM (Figure 3) and SEM (Figure 5).

4. Conclusion

This work demonstrates that periodic (passivation + deposition + etch) ASD processing can be extended to industrially relevant 45 nm half-pitch patterns and the resultant film uniformity in nanopatterns can be quantified. We leverage the unique capabilities of the DMA-TMS inhibitor to develop a passivation + deposition + etch supercycle process that greatly enhances existing selectivity and reduces LER on patterns. We report ≈8 nm of selective TiO_2 ALD with 88% uniformity and 100% selectivity on 45 nm half-pitch SiO_2/TiN line/space patterns, which is a factor of 2× improvement in TiO_2 film thickness at this scale, with lower defectivity on the pattern sidewalls, top surfaces, and corners compared to previous reports. Furthermore, we demonstrate that uniformity varies significantly with feature scale, and is expected to improve with shrinking patterns for the TiO_2 ASD process presented here. Thus, our work establishes the importance of understanding feature-dependence of uniformity to improve selectivity for electronic device-scale patterns. For the TiO_2 process described here, additional refining of the passivation, deposition, and etch parameters, including investigating nanolaminate behavior, could further improve selectivity and uniformity control on patterned substrates and 300 mm wafers. The supercycle process not only affects selectivity and uniformity, but it can also affect the composition, structure, and as such, properties of the deposited material. The TiO_2 film may be interesting for potential etch stop layer applications, but further work is required to characterize the etch properties of this film. These results are expected to extend to additional industrially relevant materials. The observational uniformity model provides a starting point for guidance on supercycle design, suggesting that higher periodicity of passivation/deposition/etch sequences will result in better selectivity and uniformity. Future work is needed to fully integrate known process parameters (e.g., growth rate, etch rate, and feature size) into the model and enable predictive capabilities for uniformity and selectivity.

5. Experimental Section

Materials and Processing: In this work, all processing steps were performed on 300 mm industry-compliant tools. Silicon oxide substrates were prepared using plasma-enhanced ALD (PEALD) to deposit 17 nm SiO_2 in an ASM Eagle 12 reactor at 75 °C on 300 mm Si(100) wafers. The resulting dielectric surface had 2.5 OH sites per nm^2.[43] For DMA-TMS exposure, a Tokyo Electron Ltd (TEL) LK-R chamber installed on a Tactras platform was first filled to 5 Torr with 500 sccm DMA-TMS and 350 Torr N_2 (DMA-TMS partial pressure = 3 Torr), as described previously.[31] Then, samples were exposed to this DMA-TMS environment for 300 s at 250 °C (resulting ≈900 Langmuir total DMA-TMS exposure). TiO_2 ALD was performed in a Polygon 8300 EmerALD chamber at 150 or 300 °C at a pressure of 5 Torr using $TiCl_4$ and H_2O. $TiCl_4$ and H_2O pulse and purge times were used that resulted in well separated, saturated reactions for TiO_2 ALD on regular flat substrates such as SiO_2. Wafers were degassed for 1 min before deposition started. TiO_2 etching occurred in a TEL T4 chamber installed on the same TEL Tactras platform as the LK-R chamber used for the passivation step. Etching was conducted by exposing the wafers to BCl_3/HBr plasma (100 W, applied to the top electrode) at 50 °C chuck temperature and a pressure of 100 mTorr. Gas flow during etching consisted of 150 standard cubic centimeters per minute(sccm) Ar, 36 sccm BCl_3, and 30 sccm HBr. For process optimization, etch rates were determined by means of TiO_2 and SiO_2 coupons (3 × 3 cm^2) glued on a SiO_2-coated 300 mm carrier wafer. Subsequent process transfer to full wafers (pattern tests) did not indicate major changes in etch rates.

Patterning: Patterns were constructed from TiN and SiO_2 lines following a previously reported procedure.[44] Briefly, this process entails physical vapor deposition of 15 nm TiN from sputtering a Ti target in N_2 ambient onto a Si wafer. Then, 75 nm SiO_2 was deposited via PEALD on top of the TiN substrate, followed by i-line immersion lithographic patterning. The final patterned structure resulted in alternating 40 nm SiO_2 lines (≈70 nm tall) with 50 nm TiN trenches, giving an overall pitch of ≈90 nm. During passivation/deposition/etch processing on these wafers, TiO_2 thicknesses were predicted based on the expected steady GPC and etch rate on blanket TiO_2 (for TiN spaces) or passivated wafers (for SiO_2 lines). For the passivated SiO_2 lines with 225 cycles deposition, the expected thickness was interpolated between the data points at 200 and 300 cycles.

Characterization: The TiO_2 films were characterized with several physical and chemical techniques. RBS was conducted using a 1.523 MeV He^+ incoming ion beam at a scattering angle of 170°, a tilt angle of 11°, and 20 nA beam current to quantify total Ti content deposited. WCA measurements were performed on a Dataphysics OCAH 230 tool using 1 µL deionized (DI) water droplets, with the average value of five measurements reported and the standard deviation used as error. Etch depth of the TiO_2 and SiO_2 layers was determined using spectroscopic ellipsometry (SE) for 5 points on a KLA Tencor F5-SCD spectroscopic ellipsometer.

XPS was used to analyze surface chemistry after passivation and etching. This was conducted in angle resolved mode using a QUANTES instrument from Physical electronics at an angle of 65° from the surface. Measurements utilized a 1486.6 eV monochromatized Al Kα X-ray source with a 100 µm spot size. Each XPS scan was calibrated to the C 1s peak at 284.8 eV. Sensitivity factors specific for each instrument were used to convert peak areas to atomic concentrations. As a result of this, it is possible that the concentrations deviate from reality in the absolute sense (generally not more than 20% relative). Unless otherwise specified, all data presented are for the 45°exit angle.

SEM was used to visualize TiO_2 growth in patterns and verify dimensions of the patterned substrates. This was performed on an FEI Helios 460 microscope with 3 kV beam energy and 0.10 nA beam current. TEM

**ADVANCED
SCIENCE NEWS**

www.advancedsciencenews.com

**ADVANCED
MATERIALS
INTERFACES**
Open Access

www.advmatinterfaces.de

was performed on a Tecnai F30 ST (FEI) tool with an FEG electron source at 300 kV in TEM mode. Prior to TEM imaging, samples were prepared with a dual beam FIB/SEM Nova600i (FEI) and Ar Ion miller PIPS (Gatan).

Supporting Information

Supporting Information is available from the Wiley Online Library or from the author.

Conflict of Interest

The authors declare no conflict of interest.

Data Availability Statement

The data that support the findings of this study are available from the corresponding author upon reasonable request.

[1] G. N. Parsons, R. D. Clark, *Chem. Mater.* **2020**, *32*, 4920.

[2] A. J. M. M. Mackus, A. A. Bol, W. M. M. Kessels, *Nanoscale* **2014**, *6*, 10941.

[3] A. C. Brummer, A. T. Mohabir, D. Aziz, M. A. Filler, E. M. Vogel, *Appl. Phys. Lett.* **2021**, *119*, 142901.

[4] T. G. Pattison, A. E. Hess, N. Arellano, N. Lanzillo, S. Nguyen, H. Bui, C. Rettner, H. Truong, A. Friz, T. Topuria, A. Fong, B. Hughes, A. T. Tek, A. DeSilva, R. D. Miller, G. G. Qiao, R. J. Wojtecki, *ACS Nano* **2020**, *14*, 4276.

[5] J.-S. Kim, G. N. Parsons, *Chem. Mater.* **2021**, *33*, 9221.

[6] S. K. Song, H. Saare, G. N. Parsons, *Chem. Mater.* **2019**, *31*, 4793.

[7] R. A. Nye, A. P. Kelliher, J. T. Gaskins, P. E. Hopkins, G. N. Parsons, *Chem. Mater.* **2020**, *32*, 1553.

[8] R. A. Nye, S. Wang, S. Uhlenbrock, J. A. I. Smythe, G. N. Parsons, *Dalton Trans.* **2022**, *51*, 1838.

[9] F. Grillo, J. Soethoudt, E. A. Marques, L. De Martín, K. Van Dongen, J. Ruud Van Ommen, A. Delabie, *Chem. Mater.* **2020**, *32*, 9560.

[10] S. E. Atanasov, B. Kalanyan, G. N. Parsons, *J. Vac. Sci. Technol., A* **2016**, *34*, 01A148.

[11] L. Lecordier, S. Herregods, S. Armini, *J. Vac. Sci. Technol., A* **2018**, *36*, 031605.

[12] R. Chen, H. Kim, P. C. McIntyre, S. F. Bent, *Chem. Mater.* **2005**, *17*, 536.

[13] J. A. Singh, N. F. W. Thissen, W.-H. Kim, H. Johnson, W. M. M. Kessels, A. A. Bol, S. F. Bent, A. J. M. Mackus, *Chem. Mater.* **2018**, *30*, 663.

[14] K. Cao, L. Shi, M. Gong, J. Cai, X. Liu, S. Chu, Y. Lang, B. Shan, R. Chen, *Small* **2017**, *13*, 1700648.

[15] J. V. Sci, S. M. George, M. Junige, S. M. George, J. V. Sci, S. M. George, M. Junige, *J. Vac. Sci. Technol., A* **2021**, *39*, 023204.

[16] J. K. Wassei, M. Mecklenburg, J. A. Torres, J. D. Fowler, B. C. Regan, R. B. Kaner, B. H. Weiller, *Small* **2012**, *8*, 1415.

[17] M. H. Park, Y. J. Jang, H. M. Sung-Suh, M. M. Sung, *Langmuir* **2004**, *20*, 2257.

[18] Z. S. Campbell, D. Jackson, J. Lustik, A. K. Al-Rashdi, J. A. Bennett, F. Li, M. Abolhasani, *RSC Adv.* **2020**, *10*, 8340.

[19] R. A. Nye, K. Van Dongen, H. Oka, D. De Simone, G. N. Parsons, A. Delabie, *J. Micro/Nanolithogr., MEMS, MOEMS* **2022**, *21*, 041407.

[20] R. A. Nye, K. Van Dongen, D. De Simone, H. Oka, G. N. Parsons, A. Delabie, *Chem. Mater.* **2022**, *35*, 2016.

[21] G. N. Parsons, *J. Vac. Sci. Technol., A* **2019**, *37*, 020911.

[22] B. Kalanyan, P. C. Lemaire, S. E. Atanasov, M. J. Ritz, G. N. Parsons, *Chem. Mater.* **2016**, *28*, 117.

[23] E. Stevens, Y. Tomczak, B. T. Chan, A. Sanchez, G. N. Parsons, A. Delabie, K. Leuven, *Chem. Mater.* **2018**, *3D*, 3223.

[24] M. J. M. Merkx, T. E. Sandoval, D. M. Hausmann, W. M. M. Kessels, A. J. M. Mackus, *Chem. Mater.* **2020**, *32*, 3335.

[25] R. Khan, B. Shong, B. G. Ko, J. K. Lee, H. Lee, J. Y. Park, I. K. Oh, S. S. Raya, H. M. Hong, K. B. Chung, E. J. Luber, Y. S. Kim, C. H. Lee, W. H. Kim, H. B. R. Lee, *Chem. Mater.* **2018**, *30*, 7603.

[26] J. Lee, J.-M. Lee, H. Oh, C. Kim, J. Kim, D. Hyun Kim, B. Shong, T. Joo Park, W.-H. Kim, J. Lee, J. Lee, T. J. Park, W. Kim, H. Oh, B. Shong, C. Kim, J. Kim, D. H. Kim, *Adv. Funct. Mater.* **2021**, *31*, 2102556.

[27] J. Yarbrough, A. B. Shearer, S. F. Bent, *J. Vac. Sci. Technol., A* **2021**, *39*, 021002.

[28] R. Chen, H. Kim, P. C. McIntyre, S. F. Bent, *Appl. Phys. Lett.* **2004**, *84*, 4017.

[29] L. L. Smith, K. Wang, G. N. Parsons, R. Hernandez, D. T. Brown, *MRS Online Proceedings Library*, Cambridge University Press, Cambridge **1999**, p. 215.

[30] J. Soethoudt, S. Crahaij, T. Conard, A. Delabie, *J. Mater. Chem. C* **2019**, *7*, 11911.

[31] J. Soethoudt, Y. Tomczak, B. Meynaerts, B. T. Chan, A. Delabie, *J. Phys. Chem. C* **2020**, *124*, 7163.

[32] W. Xu, P. C. Lemaire, K. Sharma, R. J. Gasvoda, D. M. Hausmann, S. Agarwal, *J. Vac. Sci. Technol., A* **2021**, *39*, 032402.

[33] F. Bernardoni, M. Kouba, A. Y. Fadeev, *Chem. Mater.* **2008**, *20*, 382.

[34] K. Van Dongen, R. A. Nye, J.-W. J. Clerix, C. Sixt, D. De Simone, A. Delabie, *J. Vac. Sci. Technol., A* **2023**, *41*, 032404.

[35] S. K. Song, J.-S. Kim, H. R. M. Margavio, G. N. Parsons, *ACS Nano* **2021**, *15*, 12276.

[36] M. F. J. Vos, S. N. Chopra, M. A. Verheijen, J. G. Ekerdt, S. Agarwal, W. M. M. Kessels, A. J. M. Mackus, *Chem. Mater* **2019**, *31*, 3878.

[37] M. Krishtab, S. Armini, J. Meersschaut, S. De Gendt, R. Ameloot, *ACS Appl. Mater. Interfaces* **2021**, *13*, 32381.

[38] R. A. Nye, S. K. Song, K. Van Dongen, A. Delabie, G. N. Parsons, *Appl. Phys. Lett.* **2022**, *121*, 082102.

[39] M. J. M. Merkx, A. Angelidis, A. Mameli, J. Li, P. C. Lemaire, K. Sharma, D. M. Hausmann, W. M. M. Kessels, T. E. Sandoval, A. J. M. Mackus, *J. Phys. Chem. C* **2022**, *126*, 4845.

[40] J. Y. Choi, C. F. Ahles, Y. Cho, A. Anurag, K. T. Wong, S. D. Nemani, E. Yieh, A. C. Kummel, *Appl. Surf. Sci.* **2020**, *512*, 145733.

[41] J.-W. J. Clerix, E. A. Marques, J. Soethoudt, F. Grillo, G. Pourtois, J. R. van Ommen, A. Delabie, *Adv. Mater. Interfaces* **2021**, *8*, 2100846.

[42] D. Saha, R. S. Ajimsha, K. Rajiv, C. Mukherjee, M. Gupta, M. Misra, L. M. Kukreja, *Appl. Surf. Sci.* **2014**, *315*, 116.

[43] J. Soethoudt, F. Grillo, E. A. Marques, J. R. van Ommen, Y. Tomczak, L. Nyns, S. Van Elshocht, A. Delabie, *Adv. Mater. Interfaces* **2018**, *5*, 1800870.

[44] J. Soethoudt, H. Hody, V. Spampinato, A. Franquet, B. Briggs, B. T. Chan, A. Delabie, *Adv. Mater. Interfaces* **2019**, *6*, 1900896.